doi:10.1016/j.jmb.2005.12.074 J. Mol. Biol. (2006) 357, 858–869

JMB

Available online at www.sciencedirect.com

SCIENCE DIRECT®

ELSEVIER

Crystal Structures of Human Glycerol 3-phosphate Dehydrogenase 1 (GPD1)

Xianjin Ou[1,2], Chaoneng Ji[3], Xueqing Han[2], Xiaodong Zhao[2], Xuemei Li[1,2] Yumin Mao[3] Luet-Lok Wong[4], Mark Bartlam[1,2] and Zihe Rao[1,2]*

[1]*National Laboratory of Biomacromolecules, Institute of Biophysics (IBP), Chinese Academy of Sciences, Beijing 100101, China*

[2]*"Tsinghua-IBP Joint Research Group for Structural Biology" Tsinghua University, Beijing 100084, China*

[3]*State Key Laboratory of Genetic Engineering, School of Life Sciences, Fudan University, Shanghai China*

[4]*Department of Chemistry Inorganic Chemistry Laboratory South Parks Road, Oxford OX1 3QR, United Kingdom*

**Corresponding author*

Homo sapiens L-α-glycerol-3-phosphate dehydrogenase 1 (GPD1) catalyzes the reversible biological conversion of dihydroxyacetone (DHAP) to glycerol-3-phosphate. The GPD1 protein was expressed in *Escherichia coli*, and purified as a fusion protein with glutathione *S*-transferase. Here we report the apoenzyme structure of GPD1 determined by multiwavelength anomalous diffraction phasing, and other complex structures with small molecules (NAD^+ and DHAP) by the molecular replacement method. This enzyme structure is organized into two distinct domains, the N-terminal eight-stranded β-sheet sandwich domain and the C-terminal helical substrate-binding domain. An electrophilic catalytic mechanism by the ε-NH_3^+ group of Lys204 is proposed on the basis of the structural analyses. In addition, the inhibitory effects of zinc and sulfate on GPDHs are assayed and discussed.

Keywords: L-α-glycerol-3-phosphate dehydrogenase 1; NAD-dependent dehydrogenase; crystal structure; catalytic mechanism; DHAP accumulation

Introduction

Homo sapiens L-α-glycerol-3-phosphate dehydrogenase (GPD1, EC 1.1.1.8) with 349 residues, cloned from human liver,[1] is a NAD-dependent dehydrogenase which catalyzes the reversible redox conversion of dihydroxyacetone phosphate (DHAP) and NADH to L-α-glycerol 3-phosphate (G3P) and NAD^+ (Figure 1). The reaction balance leans greatly towards the formation of G3P in physiological conditions. GPD1 is one of three isoenzymes of human glycerol 3-phosphate dehydrogenase (GPDH) exhibiting tissue-specific expression.[2] DHAP, an intermediate product of the Embden-Meyerhof glucose glycolysis pathway (EM pathway), is reduced to G3P, with the oxidation of NADH, which is mostly also generated from the EM pathway as (Figure 1). One physiological effect of this reaction is the prevention of the DHAP accumulation in organisms, which can otherwise be transformed into methylglyoxylate, a toxic compound that will specifically interact with proteins under physiological conditions.[3,4] GPDHs of the cytoplasm act in concert with the mitochondrial glycerol 3-phosphate dehydrogenase (EC 1.1.95), whose reaction balance leans in the opposite direction, to accelerate the flows of carbon sources and reducing equivalent into mitochondria. The other physiological effect is the re-oxidation of NADH to NAD^+, which will be re-used in the EM pathway to expedite the glycolysis pathway. These effects are pivotal for maintaining reductive conditions in some prokaryotic organisms, especially those whose material and energy metabolism rely strongly on the glycolysis pathway (two ATP molecules per EM pathway cycle). Taking *Trypanosoma brucei gambiense* (the cause of African sleeping sickness) as an example, GPDH is one of the first seven glycolytic enzymes[5] and is responsible for the re-oxidation of NADH to NAD^+

Abbreviations used: GPD1, L-α-glycerol-3-phosphate dehydrogenase 1; DHAP, dihydroxyacetone; GPDH, human glycerol 3-phosphate dehydrogenase.

E-mail address of the corresponding author: raozh@xtal.tsinghua.edu.cn

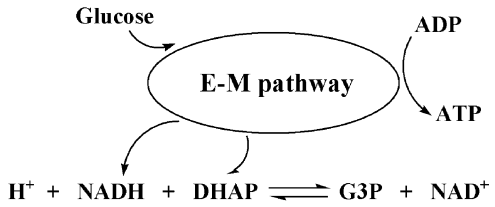

Figure 1. The reversible biochemical reaction of GPDHs.

and energy supply. It is therefore regarded as a potential target for drug design against Trypanosome-related diseases.[6,7] The structure of *Leishmania mexicana* GPDH, which shares 63% sequence identity with *T. brucei* GPDH and only 30% with human GPD1, has been determined.[8] Elucidation of the human GPD1 structure may provide a structural basis for the design of lead compounds that specifically inhibit the enzymatic activity of *Leishmania mexicana* and *Trypanosoma* GPDHs, yet leave human GPD1 unaffected.

The earlier work on GPDH from rabbit muscle, which shares 92% sequence identity with human GPD1, showed that zinc has a strong and reversible inhibition effect on GPDH enzymatic activity. The zinc inhibition is pH-dependent with an IC_{50} decreasing from 1 μM at pH 7.4 to 100 nM at pH 8.4.[9] However, the location of the zinc binding site and the mechanism of inhibition are unknown. GPDH enzymatic activity from *Trypanosoma brucei* is inhibited by sulfate ions with IC_{50} of 40 mM.[10]

Here we report the structure of the human GPD1 apoenzyme and its binary and ternary complexes with DHAP and NAD^+. The inhibitory effects of zinc and sulfate on human GPD1 were also assayed in solution. Analysis of the structures and biochemical data reveal the novel catalytic function of a conserved lysine residue (Lys204) in GPDH activity, and suggest an "open" conformation of human GPD1.

Results and Discussion

Description of the overall structure

The crystal structure of human GPD1 was solved by the multi-wavelength anomalous diffraction (MAD) method[11] and refined to an $R_{work}=21.0\%$ and $R_{free}=24.9\%$ at 2.3 Å resolution. Manual rebuilding was performed using O[12] and refinement was performed using CNS.[13] The quality of the structure was assessed using PROCHECK,[14] with 91.2% of the residues located in the most favorable region of the Ramachandran plot (Table 1). The remaining 8.8% are in additionally allowed regions and there are no residues in the generously allowed or disallowed regions. The electron density for most residues in the apoenzyme structure was well defined, except for several

Table 1. Data collection and refinement statistics

GPD1 structure	Apoenzyme	NAD^+ (co-enzyme)	DHAP	DHAP & NAD^+
Space group	$P4_32_12$	$I4_122$	$P4_32_12$	$P4_32_12$
Unit cell	$a=113.5$ Å, $b=113.5$ Å, $c=155.4$ Å, $\alpha=\beta=\gamma=90.0°$	$a=116.6$ Å, $b=116.6$ Å, $c=153.7$ Å, $\alpha=\beta=\gamma=90.0°$	$a=113.1$ Å, $b=113.1$ Å, $c=154.6$ Å, $\alpha=\beta=\gamma=90.0°$	$a=116.0$ Å, $b=116.0$ Å, $c=153.7$ Å, $\alpha=\beta=\gamma=90.0°$
Molecules per asymmetric unit	2	1	2	2
Resolution (Å)	2.3	2.6	3.0	2.45
$\langle I/\sigma(I)\rangle$	4.1 (2.3)	8.3 (2.6)	4.8 (2.0)	11.3 (3.5)
Completeness (%)	99	99.9	98	99.8
Redundancy	4.3	4.8	2.5	5.2
Phase determination	MAD	MR	MR	MR
Resolution range	50–2.3 (2.38–2.3)	50–2.6 (2.69–2.6)	50–3.0 (3.1–3.0)	50–2.45 (2.54–2.45)
R_{merge}[a] (%)	Remote: 8.4 (37.4); Peak: 8.5 (38.5); Edge: 9.0 (39)	8.0 (62.5)	8.0 (58.1)	6.3 (49.3)
R_{work}[b] (%)	21.0	18.2	23.2	22.2
R_{free}[b] (%)	24.9	23.7	28.6	26.4
Ramachandran plot[c] (%):				
Most favored	91.2	91.2	87.8	91.4
Additionally allowed	8.8	8.8	11.7	8.6
Generously allowed	0	0	0.5	0
Disallowed	0	0	0	0
RMSD bonds (Å)	0.009	0.009	0.009	0.01
RMSD angles (deg.)	1.50	1.44	1.51	1.52

Numbers in parentheses correspond to the highest resolution shell.

[a] $R_{merge}=\sum|I-\langle I\rangle|/\sum I$, where I is the observed intensity and I is the average intensity obtained from multiple observations of symmetry-related reflections.

[b] $R_{work}=\sum_{hkl}||F_o|-|F_c||/\sum_{hkl}|F_o|$. 10% of the reflections were excluded for the R_{free} calculation.

[c] Ramachandran plot was generated using the PROCHECK program: the most favored regions, additional allowed regions and generally allowed regions.

residues (-GPLGS-) added during the cloning process and a region of four residues from 125 to 128 in the C-terminal domain. The crystallographic asymmetric unit contains two monomers that form a dimer with a non-crystallographic 2-fold axis. The results of Superdex 200 gel filtration experiments also indicated the presence of a dimer in solution (data not shown). The monomer is organized into two distinct domains, an eight-stranded β-sheet sandwich domain and a C-terminal helical domain, as observed in many other structures of NAD (P)-dependent dehydrogenases (Figure 2(a)).

Monomer

The N-terminal NAD-binding domain contains a spatial actinomorphic β-sheet core composed of a six-stranded parallel β-sheet (β1–β6), with two long strand antiparallel β-sheets (β7, β8) located at the edge of this core. This β-sheet core is clamped tightly by several helices (α1–α5) on both sides to form a stable sandwich-like structure (Figure 2(a)). Interactions between the inner β-sheet core and the flanking helices of this sandwich structure are mostly mediated by hydrophobic forces. The sandwich structure of the cofactor binding domain is common to dehydrogenases, especially for NAD(P)-dependent dehydrogenases.[15] The co-enzyme, such as NAD(P), is usually bound at the edge of the β-sheet core. Another characteristic of the NAD-binding domain is the presence of the conserved GXGXXG motif in all NAD-dependent GPDHs that have been sequenced to date.[16,17] The corresponding motif in human GPD1

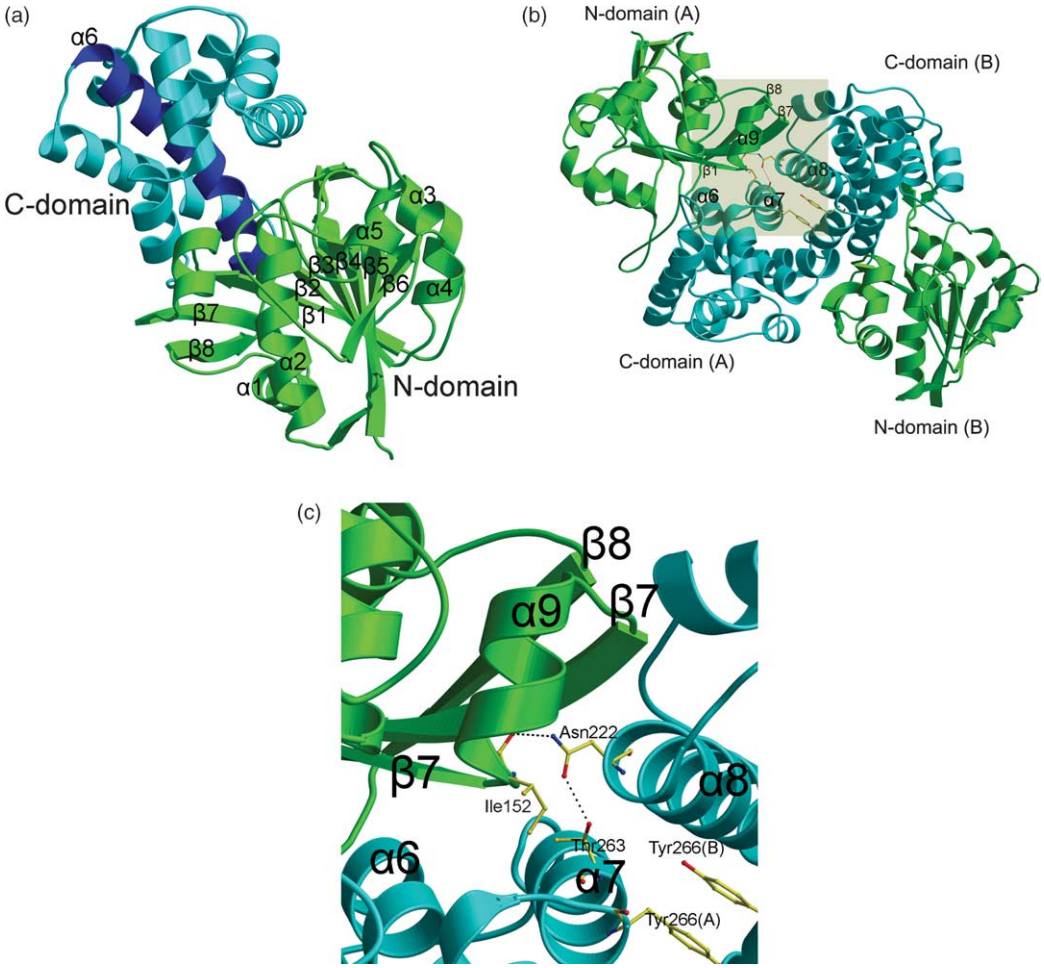

Figure 2. (a) The structure of human GPD1. The GPD1 monomer structure is shown in cartoon representation. The N-terminal eight-stranded β-sheet sandwich domain (from residues 3–190) is colored in green; the C-terminal helical substrate-binding domain (from residues 193–349) is colored in sky blue. A visible β-sheet core in the N-domain is composed by β1–β8. The NAD^+ cofactor, shown in ball-and-stick representation, binds at the periphery of the β-sheet core. The long helix α6 (from residues 193 to 202) is colored in blue. The N/C domains are connected by a three-residue turn (from residues 191 to 193) located between helix α6 and strand β8. (b) Dimer structure of human GPD1. The dimer structure of human GPD1 is shown in cartoon representation with the NAD^+ cofactor shown as ball-and-stick. There is a non-crystallographic 2-fold symmetry axis perpendicular to the center of this Figure. Residues involved in dimer formation, shown in the rectangular shadow box, are mainly located on α6, α7, β7, β8, and α8 of each monomer. (c) Detailed description of hydrogen bonds between two monomers. The conserved residue Asn222 forms two hydrogen bonds with Ile152 and Thr263 of the other monomer. Meanwhile, residues Tyr266 of each monomer are stacked in parallel.

(10-GSGNWG-15) interacts with NAD^+ directly. The C-terminal domain for the binding of DHAP or G3P substrates is mainly composed of helices. The two domains are connected by a three-residue turn (from residues 191 to 193) between strand β8 in the N-terminal domain and a long helix α6 (from residues 193 to 202) in the C-terminal domain.

Dimer

The monomers form a tightly packed dimer in the crystallographic asymmetric unit (Figure 2(b)) with no significant differences between the subunits. The root mean square deviation (RMSD) between the two monomers just is 0.24 Å for all C^α atoms. The monomer–monomer interactions are mainly hydrophobic. A total of 25 hydrogen bonds were identified between the monomers with bond distances ranging from 2.60 to 3.40 Å. A long helix α8 (from residues 220 to 241) in one monomer (Figure 2(b)) inserts into the groove composed of the strands β1 (from residues 143 to 149), β7 (from residues 161 to 168) and β8 (from residues 185 to 192), and the helix α7 (from residues 257 to 266) of the other monomer. Of the hydrogen bonds in the dimer interface, 11 are provided by helix α8 (two to Asp221, five to Asn222, one to Thr223, three to Arg229). An ordered water molecule is buried in each dimer interface by Val190, Lys178 and Glu347 (Val190 and Lys178 from one monomer; E347 from the other), forming a strong hydrogen bonding network. The phenol side-chain of Tyr266 from each molecule is within hydrophobic contact distance (3.3 Å) of the other. Asn222 (located on helix α8), conserved among 23 of the 24 GPDHs with available sequence (the only exception is GPDH from *Helicobacter pylori*, Ser), draws helix α6 and the helix α7 of the other monomer tightly together by electrostatic interactions. Glu163 in the dimer interface, also strictly conserved among 24 GPDHs, contributes two direct hydrogen bonds with the side-chain of Arg229 of the same monomer and several hydrogen bonds with residues from the other monomer *via* ordered water molecules in the dimeric interface. The large interaction area in the dimer, covering approximately 1700 $Å^2$ in each monomer, together with the high conservation of contact residues, in particular Asn222 and Glu163, suggest that GPDHs exist and function as dimers across different species.[8]

Detailed comparison reveals a high degree of structural homology between *Leishmania mexicana* GPDH and human GPD1. Residues that shape the substrate cavity are almost entirely conserved (Lys204, Asn205, Asp260, Thr264, Arg269, Asn270), with the exception of Ile152, which is substituted by Phe in *L. mexicana* GPDH. As a consequence, the design of lead compounds that specifically inhibit GPDHs of *L. mexicana* and *Trypanosoma* while leaving human GPD1 enzymatic activity unaffected, on the basis of the differences in structures of *L. mexicana* and human, is not straightforward.

Structure of binary complex with NAD^+

The binary complex of human GPD1 with NAD^+ was determined and refined to an R_{work} of 18.2% and R_{free} of 23.7% at 2.6 Å resolution (see Table 1). This complex structure is very similar to the apoenzyme structure with an RMSD of 0.93 Å for 346 C^α atoms. However, NAD^+ binding causes a seven-residue region (from residues 292 to 298) in the C-terminal domain to move by about 5 Å to form hydrogen bonds with the NAD^+ cofactor and residues in the N-domain (Figure 3(b) and (d)). At the terminals of this shifted seven-residue region are two strong interaction networks which play important roles in stabilizing the three-dimensional structure (Figure 3(c) and (d)) of both the apoenzyme and the complex with NAD^+. The first electrostatic interaction network (Figure 3(c) and (d)) occurs between Asp270, Lys296, Gln298, Glu301 of the N-domain and residues 120 to 122 and His95 of the C-domain mediated by ordered water molecules located in the interface between the N/C domains. This network anchors the following secondary-structure elements (colored in yellow, Figure 3(c)): helix α9 from 298 to 313 (anchored by Gln298 and Glu301), helix α10 from 268 to 279 (anchored by Asp270), helix α3 from 97 to 105, sheet β3 from 87 to 93 (anchored by His95) and the coil region from 120 to 122. Gln298 in the GPD1/NAD^+ holo-enzyme structure shifts by about 1.3 Å distance relative to the apoenzyme structure, contrasting with a 2.1 Å movement of Lys313 (at the C-terminal of the same helix). The other interaction network (Figure 3(c)) lies in a large hydrophobic area composed of the following residues (in red, Figure 3(c)): Val209, Phe213, Val273, Phe277, Ile284, Leu287, Leu291, Leu292 and Leu297. Structural comparison between the apo and holo-enzyme structures shows minimal movement of residues in this region. Two hydrogen bonds are observed in this shifted region (from residues 292 to 298), with the main-chain carboxyl oxygen atoms of Gly294 and Asn293 forming hydrogen bonds *via* ordered water molecules with the side-chain hydrogen oxygen of Tyr63 and the main-chain carboxyl oxygen of Lys62, respectively.

The NAD^+ cofactor is bound on the periphery of the β-sheet core of the N-terminal domain in a similar manner to that observed in structures of *L. mexicana* GPDH. The nicotinamide part of NAD^+ (Figure 3(d)) is deeply buried in the pocket between the N and C-terminal domains. All NAD-dependent GPDHs sequenced to date have the highly conserved NAD-binding motif GXGXXG,[16] and the conserved human GPD1 motif (10-GSGNWG-15) lies between strand β4 (from residues 3 to 10) and the helix α2 (from residues 14 to 27). Interactions with NAD^+ include direct hydrogen bonds formed by residues Gly12, Asn13, Trp14 Gly15, Lys120, Ala153 and Lys296, as well as hydrophobic

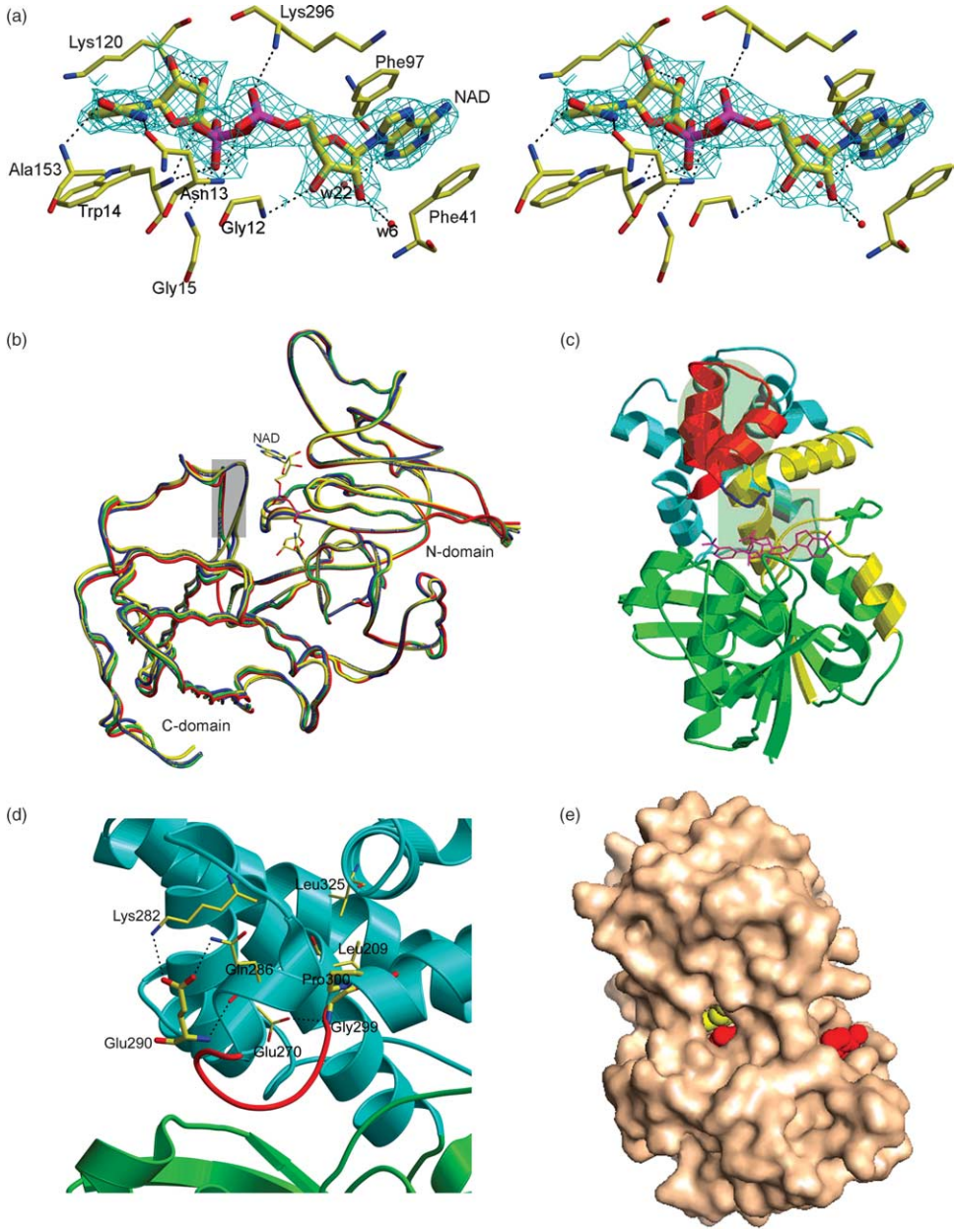

Figure 3. (a) Interaction between NAD^+ and GPD1. A stereo $2F_o - F_c$ electron density map around NAD^+ is presented at 1.0σ contour level. The hydrophobic interactions of NAD^+ with enzyme protein are shown in the two termini. 11 hydrogen bonds have been drawn in this picture, six of them are contributed directly by residues in the conserved motif 10-GSGNWG-15. (b) Main-chain superposition of the apoenzyme structure (red), structure in complex with DHAP (green), NAD^+ (blue), DHAP and NAD^+ (yellow) of human GPD1. These structures share high structural homolgy with each other except for the region from residues 292 to 298 (located in the shadow box in the picture). (c) Two anchoring networks. Residues involved in hydrophobic interaction networks are colored in red (elliptical shadow box), and those involved in hydrogen bond interactions network (rectangular shadow box) are colored in yellow. The shifted seven-residue region is colored in blue. (d) Detailed description of hydrogen bonds in the seven-residue region (from residues 292 to 298). The region shown in red undergoes a ~5 Å movement after co-enzyme binding. Residue Glu290 stands at the first fixed point, which contributes two hydrogen bonds with Lys282 and Gln286. Gly299 and Pro300 constitute the other fixed point. Pro300 is also involved in hydrophobic interactions with Leu209 and Leu325. (e) Surface representation of the ternary complex. NAD^+ and DHAP are represented in red and yellow, respectively.

interactions between the side-chain of Trp14 and the nicotinamide ring of NAD^+ (Figure 3(a)). Several water molecules are also involved in interactions with NAD^+. Hydrophobic interactions are described in Figure 3(a), and are similar to those observed in the structures of *L. mexicana*.[8] The first is the contact between the indole group of Trp14 and nicotinamide ring of NAD^+ (Figure 3(a)). Compared to the apoenzyme structure, obvious movements of the phenyl groups of Phe41 (replaced

by Met46 in *L. mexicana* GPDH) and Phe97 benefit the formation of the sandwich structure with the adenine of the bound NAD^+ (Figure 3(a)). Ser11, located in the conserved GXGXXG motif, interacts with NAD^+ *via* an ordered water molecule (not shown). The other two conserved Gly residues (Gly10 and Gly15) are located at the ends of this motif and are important for its formation.

Structure of binary complex with substrate (DHAP)

The co-crystal of GDP1 with the substrate (DHAP) was obtained from condition 15 of Crystal Screen Kit 2 (Hampton Research), and data were collected to 3.2 Å resolution. Superposition of the GPD1/DHAP complex with the apoenzyme structure and the GPD1/NAD^+ complex structures showed no significant conformational changes (Figure 3(b) and Table 2A). Electron density is strong for the phosphate group of DHAP but weak for the carbon chain tail, indicating that the DHAP phosphate group is tightly bound and mainly responsible for recognition with the enzyme active site, while the carbon tail is more mobile.

Structure of ternary complex with NAD^+ and DHAP

The ternary complex of human GPD1 with both NAD^+ (Figure 3(a)) was formed by soaking crystals of the binary complex with NAD^+. Comparisons with the other human GPD1 structures reported here show no significant changes upon substrate binding in the conformation of residues totally conserved in the active pocket (Table 2A). The main-chain RMSD between the GPD1/NAD^+ and the GPD1/DHAP/NAD^+ complex structures is 0.24 Å. It is notable that electron density for the carbon tail of DHAP in the substrate pocket appears stronger than the equivalent density in the GPD1/DHAP complex structure, indicating that the mobility of the DHAP carbon tail is restricted by the binding of NAD^+. Reflecting the electrostatic repulsion between NAD^+ and DHAP, a clear gap in electron density appears between DHAP and the nicotinamide ring of NAD^+, such that the 1-hydroxyl oxygen of DHAP is pushed forward to form a hydrogen bond with the ε-N atom of Lys120 (Figure 4).

The GPD1/DHAP/NAD^+ ternary complex enables us to delineate the putative active site. Lys120 Lys204, Asp260, Arg269, Asn270, Ile152, Asn205, Thr264 all make direct contacts with the substrate, but only the former five residues are totally conserved in all GPDHs sequenced so far; Asn205 and Thr264 are identical in 23 GPDHs but are replaced with aspartate in rabbit GPDH and serine in *Saccharomyces pombe* A, respectively.[8,18] Asp260 is located close to the active pocket between Lys120 and Lys204. Together with two other conserved residues, Thr264 and Asn205, they form a hydrogen bond interaction network (Figure 4). The distance between the 2-carbonyl oxygen atom of DHAP and ε-N atom of Lys120 is no more than 3.5 Å, suggesting a catalytic function for this residue. The C_4 atom in the nicotinamide ring, which donates a hydride ion (H^-) from NADH, or accepts one on NAD^+, is located on the other side of DHAP at a distance of 3.6 Å from C_2 of DHAP. Another unexpected discovery is the very similar and strong density consistent with a tetrahedral ion, half-encircled tightly by Arg269 observed in all crystal structures of human GPD1. This electron density is contributed by the phosphate group of DHAP in the structures containing DHAP. Considering the components of the solutions and the similar charges of sulfate and phosphate, this electron density can be interpreted as sulfate in both the structures of the apoenzyme and NAD^+-bound complex (Figure 5). Hence, the substrate/enzyme recognition should be accomplished by Arg269 and the phosphate group of the DHAP substrates, perhaps in conjunction with the interactions between the C_1 hydroxyl and the ε-N of Lys120, and the C_2 carbonyl with the ε-N of Lys204.

Table 2. Main-chain RMSD values

A. *For the apoenzyme and complex structures of human GPD1*

Structure	Apoenzyme	Ligand (DHAP)	Ligand (NAD^+)	Ligand (DHAP&NAD^+)
Apoenzyme		0.61	0.93	0.97
Ligand (DHAP)			0.72	0.76
Ligand (NAD^+)				0.24
Ligand (DHAP & NAD^+)				

B. *For the structures of L. mexicana GPDH*

PDB ID	1evy	1jdj	1m66	1m67	1n1g	1evz	1n1e
1evy		0.32	0.28	0.37	0.21	0.40	1.34
1jdj			0.21	0.31	0.29	0.36	1.34
1m66				0.27	0.21	0.36	1.32
1m67					0.34	0.32	1.23
1n1g						0.42	1.33
1evz							1.32
1n1e							

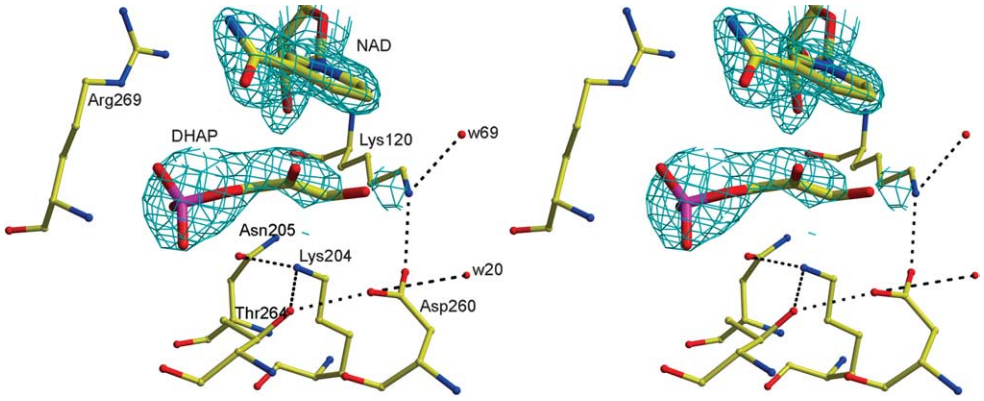

Figure 4. The putative active site. The phosphate group of DHAP is half-encircled by the side-chain of Arg269, and interacts with Arg269 and Gly268 directly by hydrogen bonds (not shown). The conserved residues Lys204, Asn205, Asp260 and Thr264 form a stable hydrogen bonding network. The other hydrogen bonding network includes residues Lys120 and Asp260, as well as an ordered water molecule (with a *B*-factor of 16.4 Å^2) which hydrogen bonds to Gly149 and Asn151 (not shown). In these two electrostatic networks, only the ε-NH^{3+} group of Lys204 is the nearest to the C_2 atom of DHAP (3.4 Å).

Sulfate occupation of the phosphate binding site is a reasonable explanation for the sulfate inhibition effect on GPD1 with a IC_{50} of 5 mM (Figure 6), similar to that reported for GPDH from rabbit muscle.[10]

Deduced open conformation of human GPD1

In the present work, we obtained many crystals from different precipitation solutions. All the crystal structures of human GPD1 reported here were determined from crystals grown from condition 15 of Crystal Screen Kit 2 (0.1 M tri-sodium citrate dihydrate (pH 5.6), 0.5 M ammonium sulfate, 1.0 M lithium sulfate monohydrate; Hampton Research). Crystals belonging to space group *C*222 were also obtained from condition 23 of Crystal Screen Kit 1 (30% PEG 400, 0.1 M Na Hepes (pH 7.5), 0.2 M $MgCl_2$; Hampton Research), and crystals belonging to space group $P2_1$ were obtained from condition 22 of Crystal Screen Kit 2 (12% PEG 20 000, 0.1 M Mes (pH 6.5); Hampton Research). However, the structures could not be solved from these different crystal forms by molecular replacement using the apoenzyme structure we determined from the $P4_32_12$ crystal form or *L. mexicana* structures as a search model. These disappointing results nevertheless suggest that there should be large conformational differences in the $P2_1$ and *C*222 crystal forms relative to the $P4_32_12$ crystal form reported here.

We note that among the *L. mexicana* GPDH apoenzyme structure (PDB code: 1EVY) and its complexes with NAD (PDB code: 1EVY), 2-fluoro-6-chloropurine (PDB code: 1JDJ), 2-bromo-6-chloropurine (PDB code: 1M66), 2-bromo-6-hydroxypurine (PDB code: 1M67), and with both NAD^+ and DHAP (PDB code:1N1E), only the ternary complex structure (PDB code: 1N1E) has a higher RMSD value with any other structure (Table 2B), which suggests a large conformational change between the 1N1E structure and others. Structural analysis of *L. mexicana* GPDH shows that the GPDH/DHAP/NAD ternary complex structure adopts a "closed" form compared to the other structures. Since there are no special components in the precipitant solution (precipitation components: 0.9 M sodium citrate, 25 mM TEA (pH 7.2), 4 mM NAD^+, 5 mM DTT, 0.2 mM EDTA and 15% (v/v) ethylene glycol) that could induce conformational changes, it is most likely that DHAP causes the substrate binding pocket to close tightly in the tertiary complex of *L. mexicana* GPDH (PDB code: 1N1E). Furthermore, given that the electron density is strong for the phosphate group of DHAP but weak for the carbon tail, it should be the phosphate group of DHAP that is mainly responsible for closing the pocket.

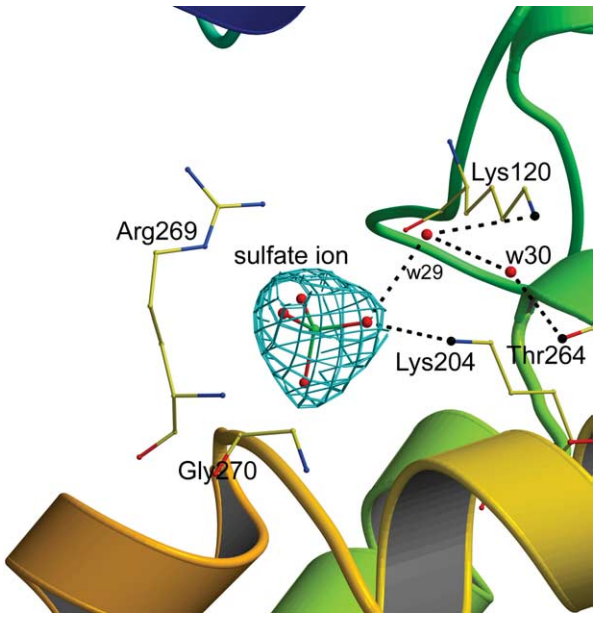

Figure 5. Sulfate ion located in the substrate pocket. Electron density omit map around the sulfate ion is shown at 1.0σ contour level.

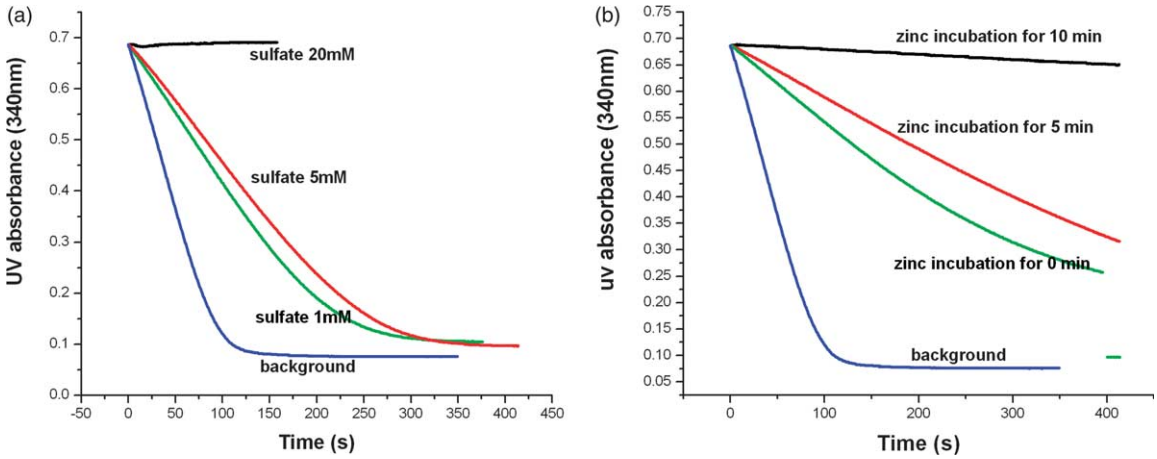

Figure 6. (a) The time-scan of enzymatic reactions with different sulfate concentrations assayed at 340 nm. The blue profile represents the background without any inhibitors. (b) The time-dependent inhibition of zinc (3 μM) on GPD1 enzymatic activity. The time-dependent inhibition was assayed at 350 mM DHAP, 226 mM NADH, and 30.5 nM GPD1 enzyme.

The frameworks of the human GPD1 structures have a higher structural similarity with the closed tertiary complex of *L. mexicana* GPDH (PDB code: 1N1E) than other structures of *L. mexicana* GPDH (Figure 7(a) and (b)). All structures of human GPD1, regardless of whether they are the apoenzyme structure or complex structures, present a closed conformation. Hence, some other factors besides DHAP must be responsible for the closed form of the apoenzyme human GPD1 structure. Considering the similarities shared by the sulfate and phosphate groups, one strong possibility is that sulfate induces the pocket to close in structures of human GPD1. Consistent with this proposal, the Hampton Research Crystal Screen kit 1-23 and kit 2-22 crystallization conditions do not contain sulfate whereas kit 2-15 (used to grow the $P4_32_12$ crystals) does. This might explain why it was not possible to solve the structure from crystals from the first two conditions using the structure solved from crystals grown using kit 2-15 as a search model. In addition, this hypothesis is confirmed by enzymatic data showing that the enzyme activity is completely inhibited by 20 mM sulfate (Figure 6(a)).

In conclusion, GPD1 should present an open form if there is no sulfate or phosphate in the solution. A large conformational change would occur when the DHAP substrate or sulfate binds to the enzyme. Such conformational changes between different domains upon the binding of the substrate or/and cofactor binding have previously been observed in a number of dehydrogenases, including glutamate dehydrogenase,[19,20] liver alcohol dehydrogenase,[21] and glyceraldehyde-3-phosphate dehydrogenase.[22]

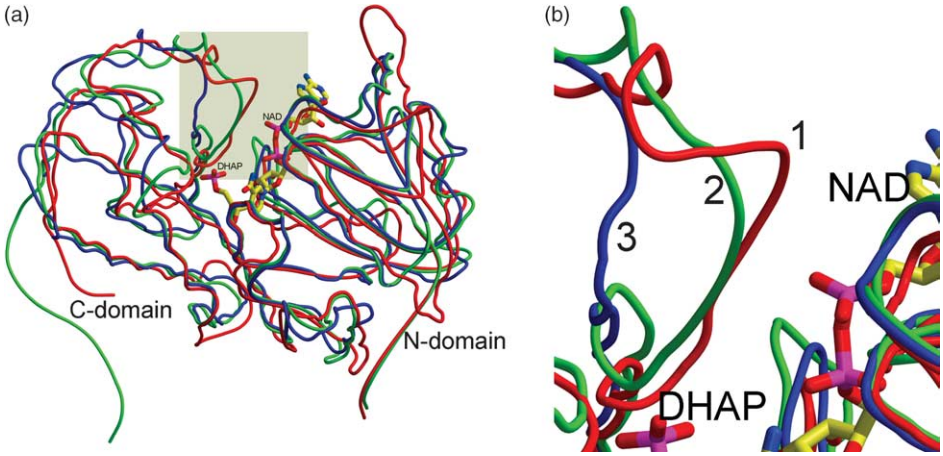

Figure 7. (a) and (b) Superposition of the human GPD1 apoenzyme structure (red) with the *L. mexicana* GPDH structures in complex with NAD (blue, PDB code: 1EVZ), and in complex with both NAD and DHAP (green, PDB code: 1N1E). (b) An enlarged image of the shaded area in (a). The structure of human apo-GPD1 is structurally closer to the 1N1E structure (closed form) of *L. mexicana* than the 1EVZ structure (open form) of *L. mexicana*.

The proposed catalytic mechanism for GPDH

The crystal structures of human GPD1 determined here, together with the reported structures of *L. mexicana* GPDH and functional study data, provide a firm basis for assessing the catalytic mechanism of GPDHs. Among the highly conserved residues that define the active site, Arg269 has been shown to be important for substrate recognition from the structures reported here. Lys204, Asn205, Asp260 and Thr264 form a hydrogen bonding network centered on Lys204 (Figure 4). This arrangement shows little movement among all structures of human GPD1 reported here. The side-chain carboxyl oxygen atoms of Asn205 and Asp260 are 4.2 and 4.8 Å respectively from the C_2 atom of DHAP. The side-chain hydroxyl of Thr264 is 4.5 Å and the ε-N of Lys204 is no more than 3.5 Å from the C_2 carbonyl oxygen of the DHAP substrate. Another hydrogen bonding network consisting of Lys120, the side-chain oxygen of Asp260 and an ordered water molecule is observed in all structures (Figure 4), and assists substrate recognition *via* a hydrogen bond between the 1-hydroxyl group of DHAP and the ε-N atom of Lys120. These data suggest that the substrate recognition interactions are highly conserved in all 24 GPDHs with known sequence. From the work by Maret and colleagues on rabbit muscle GPDH, the k_{cat}/k_m for the reaction of DHAP and NADH decreases from 4 $\mu M^{-1}\,s^{-1}$ at pH 7.0 to 0.1 $\mu M^{-1}\,s^{-1}$ at pH 9.0; whereas, k_{cat}/k_m for G3P oxidation by

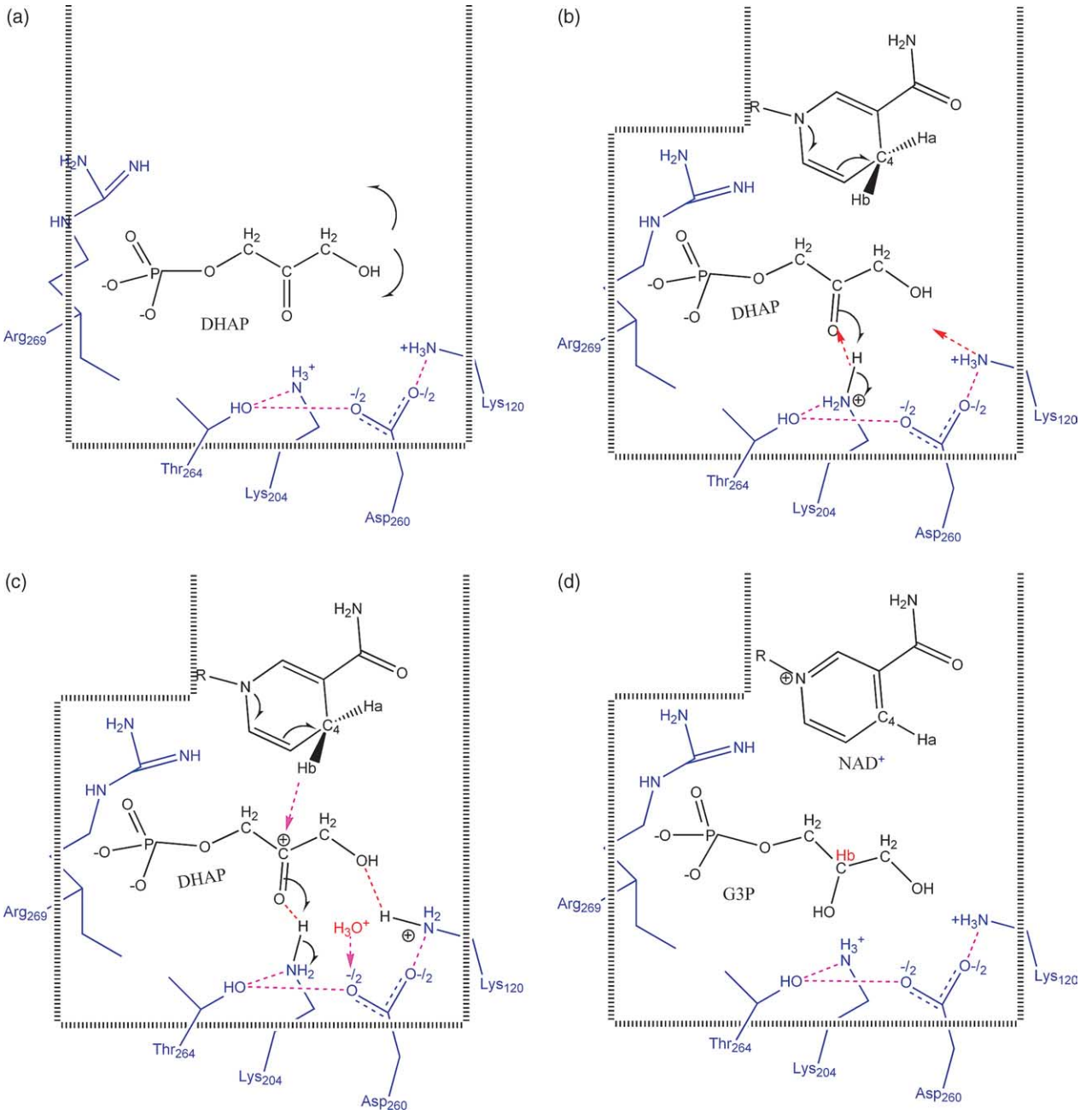

Scheme 1.

NAD^+ increases from 0.1 $\mu M^{-1} s^{-1}$ at pH 7.0 to 1.5 $\mu M^{-1} s^{-1}$ at pH 9.0.[9] Hence, alkaline pH retards the conversion of DHAP to G3P and promotes the reverse reaction.

On the basis of the structural and biochemical evidence, we propose a unifying mechanism for GPDHs as shown in scheme 1. In the absence of substrate or sulfate or phosphate ions, the enzyme is in an open conformation. Binding of the DHAP substrate, in particular the recognition between the phosphate group and Arg269, causes the active site to close around the substrate, but the substrate carbon chain remains mobile. The binding of the NAD(H) cofactor tightens the substrate pocket, the hydrogen bond between the C_2 carbonyl oxygen and ε-NH_3^+ of Lys204 is strengthened, and the 1-hydroxyl of the substrate is fixed by a hydrogen bond with Lys120. The crucial role of Lys204 then becomes evident. At pH 7.0, the ε-NH_2 atom of Lys204 is protonated and forms a hydrogen bond with the C_2 carbonyl oxygen, thus polarizing the carboxyl group and promoting nucleophilic attack by the hydride of NADH on the C_2 carbon. The tetrahedral oxyanion then abstracts a proton from the ε-NH_3^+ to form the G3P product. At alkaline pH (9.0), the ε-N atom of Lys204 may be neutral and accept a hydrogen bond from the C_2–OH of G3P. The build-up of negative charge on the oxygen facilitates the hydride ion (H^-) transfer from G3P to the NAD^+ cofactor. The reverse reaction (DHAP formation) cycle is completed by proton transfer from the C_2–OH of G3P to ε-NH_2 of Lys204. The protonation state of Lys204, which is conserved among GPDHs, controls the equilibrium position.

Zinc and sulfate inhibition of GPD1

Atomic absorption spectroscopy experiments were carried out at pH 6.0 and 9.0 to confirm the zinc binding to GPD1 protein in Tris–HCl buffer (instrument: ICP-AES vista-MPX). The zinc content, measured in the GPD1 enzyme at pH 6.0, is 0.0241 mg/ml compared with 0.0236 mg/ml in the buffer background. At pH 9.0, the zinc content is 0.10 mg/ml compared to 0.013 mg/ml of buffer background; the zinc concentration ((0.10–0.013)/65.38 = 1.33 μM) is almost the same as the concentration of GPD1 (1.32 μM) assayed by 280 nm UV absorption. These results suggest that zinc binds to GPD1 more tightly at alkaline pH, with one protein molecule bound by one zinc ion. All crystals were obtained at pH 5.6 and no zinc ion could be observed in the crystal structure after soaking in a solution of zinc sulfate. At pH 7.5, the remaining enzymatic activities (according to the initial reaction velocity) after incubation with $ZnCl_2$ added to solution A (DHAP and GPD1) for 0 min, 5 min and 10 min, are 30.4%, 21.7% and 2%, respectively, suggesting a strong inhibitory effect (Figure 6(b)).

Compared with zinc inhibition, the sulfate ion shows a weaker but more rapid inhibitory effect on GPD1 (Figure 6(a)). The GPD1 enzyme activity is not sensitive to sulfate in the concentration range from 1 mM to 5 mM, and their remaining activities are 56.5% and 43.5%. However, total enzymatic activity is quickly lost with 20 mM Na_2SO_4.

Conclusions

From the structure of the apoenzyme form of human GPD1, its binary complex structures with DHAP and NAD^+ and its ternary complex structure with both DHAP and NAD^+, we have identified the key residue for initial recognition of the substrate (Arg269), that of cofactor binding and proposed a unifying mechanism for GPDH activity with a key role for the ε-NH_2 group of the conserved residue Lys204. We have also deduced an open form of human GPD1 in the absence of substrate, sulfate or phosphate ions on the basis of structural comparison.

Materials and Methods

Cloning, expression and purification

The cloning, expression, purification and preliminary crystallographic studies of human GPD1 will be described elsewhere. Briefly, the human GPD1 gene carried on a plasmid (provided by Chaoneng Ji) between the BamHI and XhoI endonuclease sites was amplified by polymerase chain reaction, sub-cloned into the pGEX-6p-1 vector (Amersham Biosciences), and expressed in *E. coli* BL-21 DE3. The protein was purified by GST affinity chromatography, followed by gel filtration chromatography. The production of the selenomethionyl-GPD1 derivative was similar to that of the apoenzyme protein with several modifications, and will be described elsewhere. The purified protein sample was dialyzed against a buffer of 150 mM NaCl in 50 mM Tris–Cl (pH 7.0).

Crystallization and data collection

The hanging-drop vapor-diffusion method was used for screening for crystallization conditions with commercial screening kits (Hampton Research) by mixing 1 μl of protein at concentration 5, 15, 30, and 60 mg/ml with an equal volume of precipitant solution at 16 °C. The optimum crystals (octahedron-like) were obtained from condition 15 of Crystal Screen kit II (0.1 M tri-sodium citrate dihydrate (pH 5.6), 0.5 M ammonium sulfate, 1.0 M lithium sulfate monohydrate) at concentrations ranging from 10 mg/ml to 60 mg/ml. Diffraction data were collected at the Beijing Synchrotron Radiation Facility (BSRF, Institute of High Energy Physics, Beijing, China). The data frames were indexed and integrated with DENZO and merged with SCALEPACK.[23] The crystals belong to the $P4_32_12$ space group with unit cell parameters $a = b = 113.9$ Å, 113.9 Å, $c = 155.4$ Å. Calculations with the program CNS[13] showed that five selenium sites are located in one molecule from Patterson maps. There are two molecules in each asymmetric unit with a crystal solvent content of 63%.

Structures of the binary and ternary complexes of human GPD1 with DHAP and NAD^+ were determined

by molecular replacement (MR) methods with the program CNS[13] using the apoenzyme structure of human GPD1 as a search model, from crystals soaked in well solutions containing the relevant compounds. Data collection and structure refinement statistics are shown in Table 1.

Enzyme activity assays

Enzyme activity assays were performed spectrophotometrically at 340 nm in the direction of NADH in Tris–HCl buffer (50 mM NaCl, 150 mM Tris (pH 7.5), 0.2 mM EDTA); the extinction coefficient at 340 nm is 6220. GPD1 protein was purified to 90% measured by SDS-polyacrylamide gel electrophoresis. DHAP (dilithium salt) was purchased from SIGMA. Enzymatic reactions were started upon mixing solution A (containing DHAP and enzyme) with solution B (containing NADH and $ZnCl_2$ or Na_2SO_4) at 25 °C. The concentrations of enzyme protein and NADH were invariable at 30 nM and 226 μM, respectively. All initial enzymatic velocities were calculated within the first 50 s. One enzymatic activity unit is defined as the amount of enzyme that converts 1 μM of substrate (DHAP) per min at 25 °C.

Protein Data Bank accession codes

The coordinates and structure factors for human GPD1 have been deposited in the Protein Data Bank (PDB) with accession number 1X0V. The coordinates and structure factors for the human GPD1/NAD binary complex have been deposited in the PDB with accession number 1X0X. The coordinates and structure factors for the human GPD1/DHAP/NAD ternary complex have been deposited in the PDB with accession number 1WPQ.

Acknowledgements

We are grateful to Yiwei Liu, Zhiyong Lou, Fei Sun, Sheng Ye, Yi Ding, and Feng Xu for technical assistance. We thank Peng Liu and Yuhui Dong (BSRF) for their help with data collection. This study was supported by the Ministry of Science & Technology (MOST) Human Liver Proteomics Project (grant no. 2004CB520801), "863" Project (grant no. 2002BA711A12), "973" Project (grant no. G1999075602) and the NSFC (grant no. 30221003).

References

1. Menaya, J., Gonzalez-Manchon, C., Parrilla, R. & Ayuso, M. S. (1995). Molecular cloning, sequencing and expression of a cDNA encoding a human liver NAD-dependent alpha-glycerol-3-phosphate dehydrogenase. *Biochim. Biophys. Acta*, **1262**, 91–94.
2. Hopkinson, D. A., Peters, J. & Harris, H. (1974). Rare electrophoretic variants of glycerol-3-phosphate dehydrogenase: evidence for two structural gene loci (GPD1 and GPD2). *Ann. Hum. Genet.* **37**, 477–484.
3. Lo, T. W., Westwood, M. E., McLellan, A. C., Selwood, T. & Thornalley, P. J. (1994). Binding and modification of proteins by methylglyoxal under physiological conditions. A kinetic and mechanistic study with N alpha-acetylarginine, N alpha-acetylcysteine, and N alpha-acetyllysine, and bovine serum albumin. *J. Biol. Chem.* **269**, 32299–32305.
4. Denise, H., Giroud, C., Barrett, M. P. & Baltz, T. (1999). Affinity chromatography using trypanocidal arsenical drugs identifies a specific interaction between glycerol-3-phosphate dehydrogenase from *Trypanosoma brucei* and Cymelarsan. *Eur. J. Biochem.* **259**, 339–346.
5. Opperdoes, F. R. & Borst, P. (1977). Localization of nine glycolytic enzymes in a microbody-like organelle in *Trypanosoma brucei*: the glycosome. *FEBS Letters*, **80**, 360–364.
6. Aronov, A. M., Suresh, S., Buckner, F. S., Van Voorhis, W. C., Verlinde, C. L., Opperdoes, F. R. *et al*. (1999). Structure-based design of submicromolar, biologically active inhibitors of trypanosomatid glyceraldehyde-3-phosphate dehydrogenase. *Proc. Natl Acad. Sci. USA*, **96**, 4273–4278.
7. Eisenthal, R. & Cornish-Bowden, A. (1998). Prospects for antiparasitic drugs. The case of *Trypanosoma brucei*, the causative agent of African sleeping sickness. *J. Biol. Chem.* **273**, 5500–5505.
8. Suresh, S., Turley, S., Opperdoes, F. R., Michels, P. A. & Hol, W. G. (2000). A potential target enzyme for trypanocidal drugs revealed by the crystal structure of NAD-dependent glycerol-3-phosphate dehydrogenase from *Leishmania mexicana*. *Struct. Fold. Des.* **8**, 541–552.
9. Maret, W., Yetman, C. A. & Jiang, L. (2001). Enzyme regulation by reversible zinc inhibition: glycerol phosphate dehydrogenase as an example. *Chem. Biol. Interact.* **130-132**, 891–901.
10. Marche, S., Michels, P. A. & Opperdoes, F. R. (2000). Comparative study of *Leishmania mexicana* and *Trypanosoma brucei* NAD-dependent glycerol-3-phosphate dehydrogenase. *Mol. Biochem. Parasitol.* **106**, 83–91.
11. Hendrickson, W. A. & Ogata, C. M. (1997). Phase determination from multiwavelength anomalous diffraction measurements. *Methods Enzymol.* **276**, 494–523.
12. Jones, T. A., Zou, J. Y., Cowan, S. W. & Kjeldgaard, M. (1991). Improved methods for building protein models in electron density maps and the location of errors in these models. *Acta Crystallog. sect. A*, **47**, 110–119.
13. Brunger, A. T., Adams, P. D., Clore, G. M., DeLano, W. L., Gros, P., Grosse-Kunstleve, R. W. *et al*. (1998). Crystallography & NMR system: a new software suite for macromolecular structure determination. *Acta Crystallog. sect. D*, **54**, 905–921.
14. Laskowski, R. A., MacArthur, M. W., Moss, D. S. & Thornton, J. M. (1993). PROCHECK: a program to check the stereochemical quality of protein structures. *J. Appl. Crystallog.* **26**, 283–291.
15. Rossmann, M. G. & Liljas, A. (1975). Evolutionary and structural relationships among dehydrogenases. In *The Enzymes* (Boyer, P. D., ed.), pp. 61–102, Academic Press, New York.
16. Wierenga, R. K., Terpstra, P. & Hol, W. G. (1986). Prediction of the occurrence of the ADP-binding beta alpha beta-fold in proteins, using an amino acid sequence fingerprint. *J. Mol. Biol.* **187**, 101–107.
17. Carugo, O. & Argos, P. (1997). NADP-dependent enzymes. I: Conserved stereochemistry of cofactor binding. *Proteins: Struct. Funct. Genet.* **28**, 10–28.

18. Otto, J., Argos, P. & Rossmann, M. G. (1980). Prediction of secondary structural elements in glycerol-3-phosphate dehydrogenase by comparison with other dehydrogenases. *Eur. J. Biochem.* **109**, 325–330.
19. Stillman, T. J., Baker, P. J., Britton, K. L. & Rice, D. W. (1993). Conformational flexibility in glutamate dehydrogenase. Role of water in substrate recognition and catalysis. *J. Mol. Biol.* **234**, 1131–1139.
20. Stillman, T. J., Migueis, A. M., Wang, X. G., Baker, P. J., Britton, K. L., Engel, P. C. & Rice, D. W. (1999). Insights into the mechanism of domain closure and substrate specificity of glutamate dehydrogenase from *Clostridium symbiosum*. *J. Mol. Biol.* **285**, 875–885.
21. Colonna-Cesari, F., Perahia, D., Karplus, M., Eklund, H., Braden, C. I. & Tapia, O. (1986). Interdomain motion in liver alcohol dehydrogenase. Structural and energetic analysis of the hinge bending mode. *J. Biol. Chem.* **261**, 15273–15280.
22. Skarzynski, T. & Wonacott, A. J. (1988). Coenzyme-induced conformational changes in glyceraldehyde-3-phosphate dehydrogenase from *Bacillus stearothermophilus*. *J. Mol. Biol.* **203**, 1097–1118.
23. Otwinowski, Z. & Minor, W. (1997). Processing of X-ray diffraction data collected in oscillation mode. In *Macromolecular Crystallography* (Carter, C. W., Jr & Sweet, R. M., eds), part A, vol. 276, pp. 307–326, Academic Press, New York.

Edited by R. Huber

(Received 22 September 2005; received in revised form 19 December 2005; accepted 23 December 2005)
Available online 18 January 2006